

## Supporting information

# Molten salt strategy and plasma technology induced MnO<sub>2</sub> with oxygen vacancy for high performance Zn-ions battery

Fuqiang Shao<sup>1</sup>, Shuke Li<sup>1</sup>, Yanchao Xu<sup>1</sup>, Yang Jiao<sup>1\*</sup>, Jianrong Chen<sup>1\*</sup>

**\*Corresponding author:** E-mail: [yangjiao@zjnu.edu.cn](mailto:yangjiao@zjnu.edu.cn) and [cjr@zjnu.cn](mailto:cjr@zjnu.cn), **Phone:** (+86)-0579-82291275

1 College of Geography and Environmental Sciences, Zhejiang Normal University,  
Jinhua, 321004, China

## Calculation

According to the reported literature<sup>1, 2</sup>, the current ( $i$ ) and scan rate ( $v$ ) in CV curves have relationships with equation:

$$i = av^b \quad (1)$$

$$\lg(i) = b\lg(v) + \lg(a) \quad (2)$$

where  $i$  is peak current,  $a$  correspond to constant,  $v$  is the scan rate and  $b$  is equaled to the slope of the  $\lg(v)$ - $\lg(i)$  plots. If  $b$  approximately equals to 0.5, suggests the diffusion process is dominant, while a capacitive behavior will dominate when  $b$  is about 1<sup>3</sup>.

The contribution ratios of the two processes at scan rates from 0.1 to 0.5 mV s<sup>-1</sup> can be calculated by equations (3):

$$i(v) = k_1v + k_2v^{1/2} \quad (3)$$

where  $k_1v$  and  $k_2v^{1/2}$  corresponds to the current contributions originating from the surface capacitive effects and the diffusion-controlled insertion processes, respectively. By determining the values of  $k_1$  and  $k_2$ , we can further analysis contribution ratios between diffusion-controlled process and capacitive effects at different scan rates. The Eq. (3) can be changed as follows:

$$i(v)/v^{1/2} = k_1v^{1/2} + k_2 \quad (4)$$

The values of  $k_1$  and  $k_2$  can be obtained from the slope and y intercept of the linear fit of the plot of  $i(v)/v^{1/2}$  versus  $v^{1/2}$ , respectively. The capacitive and diffusion-controlled currents assistance to the total charge was separately calculated by inserting the values of  $k_1$  and  $k_2$  into the Eq. (4).

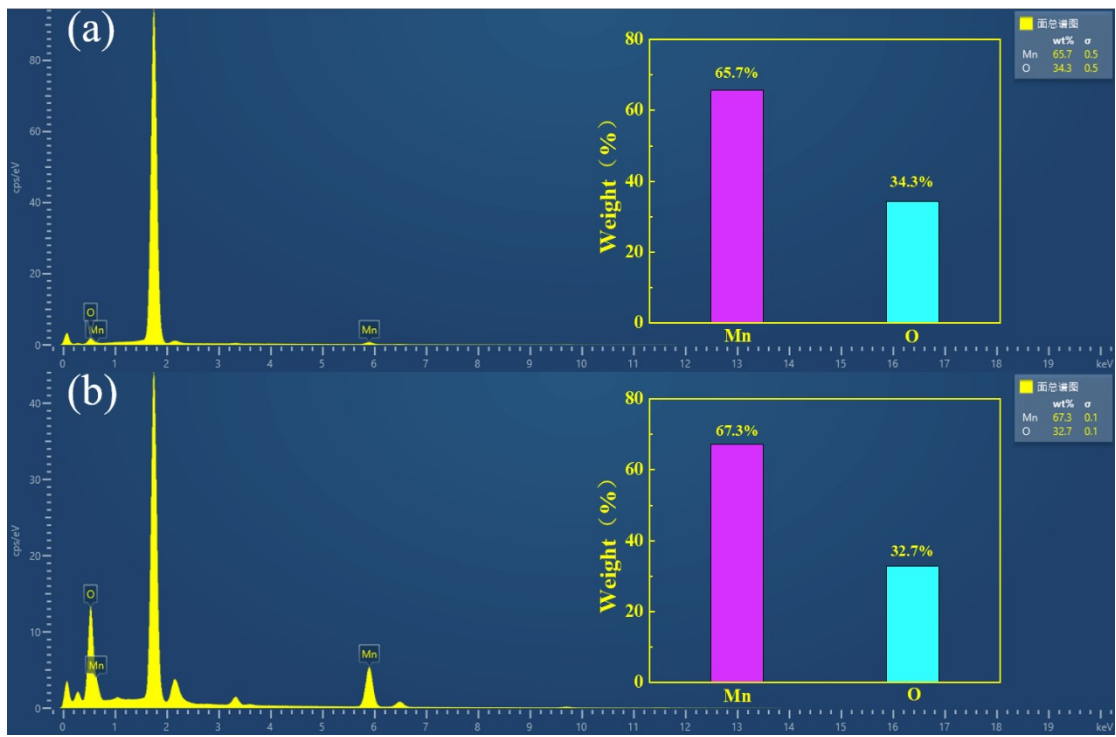


**Figure S1.** Elemental composition analysis of (a) MnO<sub>2</sub> and (b) MnO<sub>2</sub>-3.

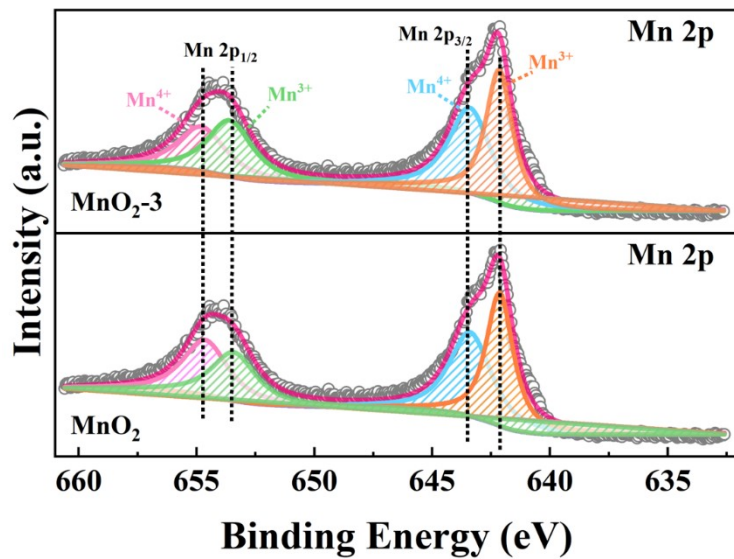


**Figure S2.** Mn 2p XPS spectra comparison of MnO<sub>2</sub> and MnO<sub>2</sub>-3.

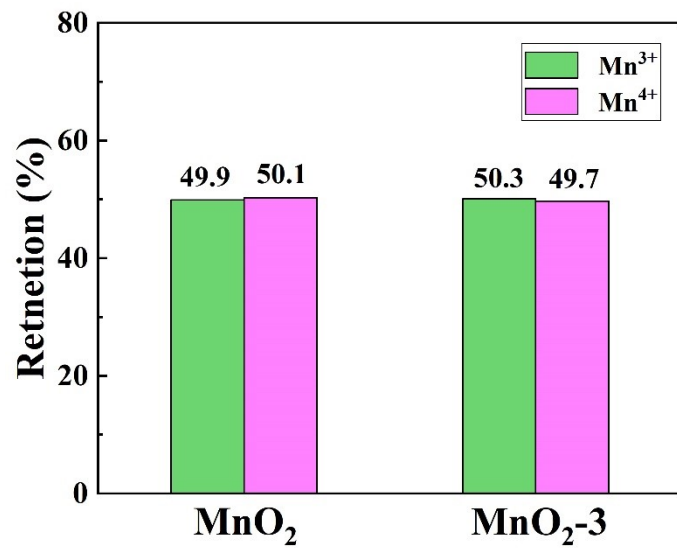


**Figure S3.** quantitatively statistics of the percentage of  $\text{Mn}^{3+}$  and  $\text{Mn}^{4+}$  in the samples.

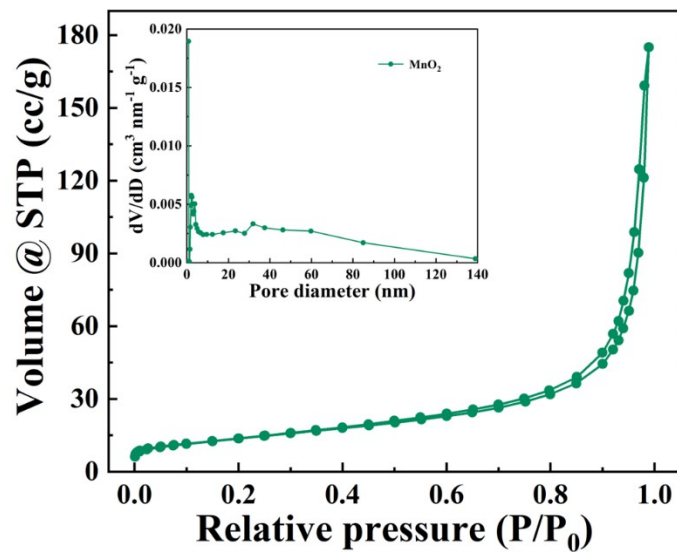


**Figure S4.** Nitrogen adsorption-desorption isotherm and pore distribution of  $\text{MnO}_2$ .

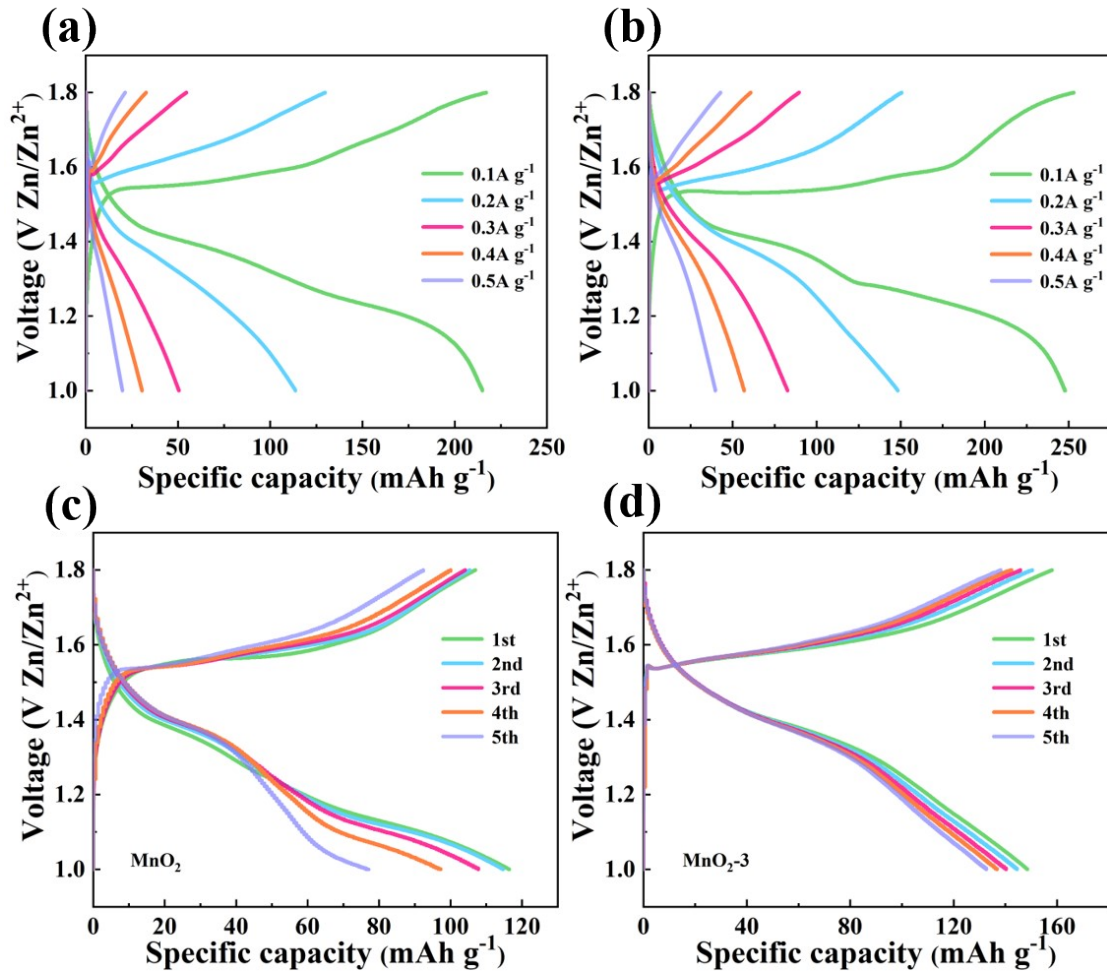


**Figure S5.** GCD curves at current densities from  $0.1$  to  $0.5 \text{ A g}^{-1}$  of (a)  $\text{MnO}_2$  and (b)  $\text{MnO}_2\text{-}3$ .

GCD profiles in the initial 5 cycles of (c)  $\text{MnO}_2$  and (d)  $\text{MnO}_2\text{-}3$ .

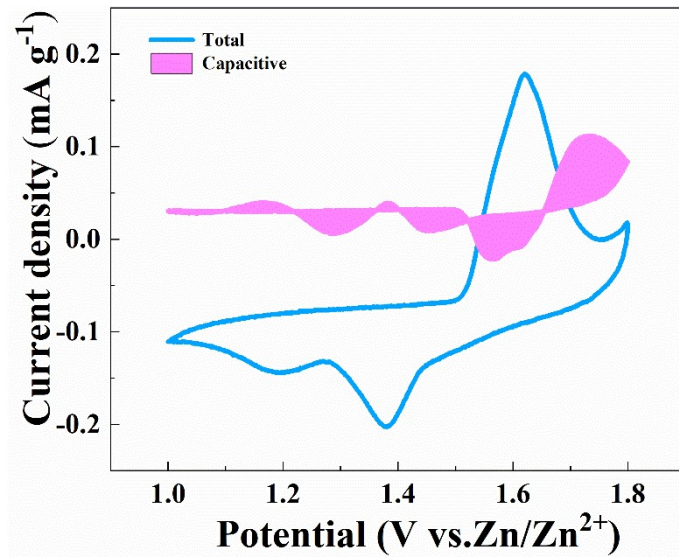


**Figure S6.** Capacitive and diffusion-controlled contribution analysis of the CV curves of  $\text{MnO}_2\text{-}3$ .

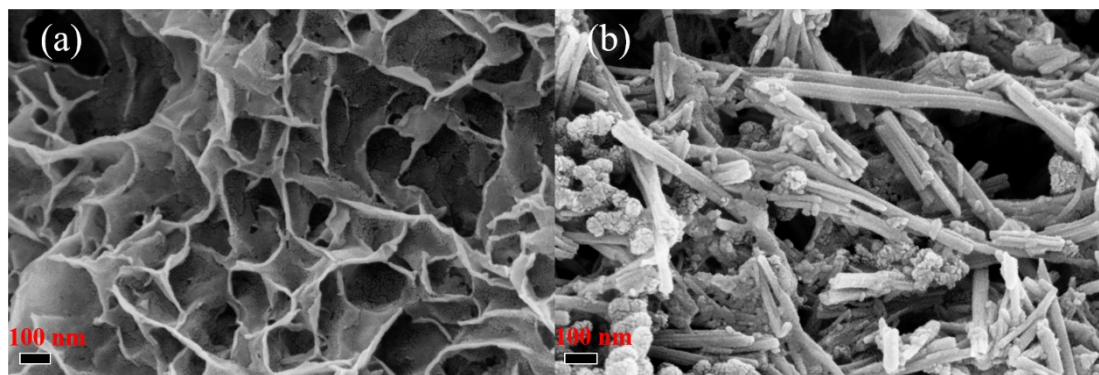


**Figure S7.** SEM images of (a)  $\text{MnO}_2$  and (b)  $\text{MnO}_2\text{-}3$  after 10 cycles.

**Table S1.** Comparison of electrochemical performance of other materials

Materials	Specific capacity (mA h g <sup>-1</sup> )	Cycle number	Capacity retention	Reference
$\delta$ -MnO <sub>2</sub>	170 (0.1A g <sup>-1</sup> )	100 (0.1 A g <sup>-1</sup> )	83%	<sup>4</sup>
$\alpha$ -MnO <sub>2</sub> @PPy	137 (0.1A g <sup>-1</sup> )	100 (0.1 A g <sup>-1</sup> )	58%	<sup>5</sup>
$\alpha$ -MnO <sub>2</sub>	180 (42 mA g <sup>-1</sup> )	30 (42 mA g <sup>-1</sup> )	76%	<sup>6</sup>
$\delta$ -MnO <sub>2</sub>	252 (82 mA g <sup>-1</sup> )	100 (83 mA g <sup>-1</sup> )	44%	<sup>7</sup>
$\delta$ -MnO <sub>2</sub>	108 (12.3 mA g <sup>-1</sup> )	125 (12.3 mA g <sup>-1</sup> )	63%	<sup>8</sup>
UCT-1-250	222 (0.1A g <sup>-1</sup> )	200 (0.1A g <sup>-1</sup> )	57%	<sup>9</sup>
$\gamma$ - MnO <sub>2</sub>	250 (0.5 mA cm <sup>-2</sup> )	40 (0.5 mA cm <sup>-2</sup> )	63%	<sup>10</sup>
<b>This work</b>	<b>252 (0.1A g<sup>-1</sup>)</b>	<b>100 (0.2A g<sup>-1</sup>)</b>	<b>81%</b>	

## References

1. S. Xiong, M. Lin, L. Wang, S. Liu, S. Weng, S. Jiang, Y. Xu, Y. Jiao and J. Chen, *Applied Surface Science*, 2021, **546**.
2. S. Zhang, S. Long, H. Li and Q. Xu, *Chemical Engineering Journal*, 2020, **400**.
3. J. Long, F. Yang, J. Cuan, J. Wu, Z. Yang, H. Jiang, R. Song, W. Song, J. Mao and Z. Guo, *ACS Appl Mater Interfaces*, 2020, **12**, 32526-32535.
4. C. Guo, H. Liu, J. Li, Z. Hou, J. Liang, J. Zhou, Y. Zhu and Y. Qian, *Electrochimica Acta*, 2019, **304**, 370-377.
5. C. Guo, S. Tian, B. Chen, H. Liu and J. Li, *Materials Letters*, 2020, **262**.
6. B. Lee, H. R. Lee, H. Kim, K. Y. Chung, B. W. Cho and S. H. Oh, *Chem Commun (Camb)*, 2015, **51**, 9265-9268.
7. M. H. Alfaruqi, J. Gim, S. Kim, J. Song, D. T. Pham, J. Jo, Z. Xiu, V. Mathew and J. Kim, *Electrochemistry Communications*, 2015, **60**, 121-125.
8. S.-D. Han, S. Kim, D. Li, V. Petkov, H. D. Yoo, P. J. Phillips, H. Wang, J. J. Kim, K. L. More, B. Key, R. F. Klie, J. Cabana, V. R. Stamenkovic, T. T. Fister, N. M. Markovic, A. K. Burrell, S. Tepavcevic and J. T. Vaughey, *Chemistry of Materials*, 2017, **29**, 4874-4884.
9. Y. Wu, J. Fee, Z. Tobin, A. Shirazi-Amin, P. Kerns, S. Dissanayake, A. Mirich and S. L. Suib, *ACS Applied Energy Materials*, 2020, **3**, 1627-1633.
10. M. H. Alfaruqi, V. Mathew, J. Gim, S. Kim, J. Song, J. P. Baboo, S. H. Choi and J. Kim, *Chemistry of Materials*, 2015, **27**, 3609-3620.